Variations of tropical upper tropospheric clouds with sea surface temperature and implications for radiative effects

Hui Su, Jonathan H. Jiang, Yu Gu[1], J. David Neelin[1], Brian H. Kahn, Daniel Feldman[2], Yuk L. Yung[2], Joe W. Waters, Nathaniel J. Livesey, Michelle L. Santee, William G. Read

Jet Propulsion Laboratory, California Institute of Technology, Pasadena, California, 91109, USA

[1]Department of Atmospheric and Oceanic Sciences, University of California, Los Angeles, CA 90095, USA.

[2]Division of Geological and Planetary Sciences, California Institute of Technology, Pasadena, CA, 91125, USA

Hui Su, M/S 183-701, Jet Propulsion Laboratory, California Institute of Technology, 4800 Oak Grove Drive, Pasadena, California 91109-8099, U.S.A.

(Email: Hui.Su@jpl.nasa.gov)

Abstract. The variations of tropical upper tropospheric (UT) clouds with sea surface temperature (SST) are analyzed using effective cloud fraction from the Atmospheric Infrared Sounder (AIRS) on Aqua and ice water content (IWC) from the Microwave Limb Sounder (MLS) on Aura. The analyses are limited to UT clouds above 300 hPa. Our analyses do not suggest a negative correlation of tropical-mean UT cloud fraction with the cloud-weighted SST (CWT). Instead, both tropical-mean UT cloud fraction and IWC are found to increase with CWT, although their correlations with CWT are rather weak. The rate of increase of UT cloud fraction with CWT is comparable to that of precipitation, while the UT IWC and ice water path (IWP) increase more strongly with CWT. The radiative effect of UT clouds is investigated, and they are shown to provide a net warming at the top of the atmosphere. An increase of IWP with SST yields an increase of net warming that corresponds to a positive feedback, until the UT IWP exceeds a value about 50% greater than presently observed by MLS. Further increases of the UT IWP would favor the shortwave cooling effect, causing a negative feedback. Sensitivities of UT cloud forcing to the uncertainties in UT CFR and IWC measurements are discussed.

1. Introduction

High-altitude clouds have important radiative effects on the Earth-atmosphere system. They are closely related to upper tropospheric humidity (UTH), which is the dominant contributor to the greenhouse effect [e.g. *Betts*, 1990; *Lindzen*, 1990; *Sun and Lindzen*, 1993; *Udelhofen and Hartmann*, 1995; *Soden and Fu*, 1995; *Su et al.*, 2006a]. They also provide significant radiative forcing to the climate system in their own right. Their net radiative effect results from a balance between warming from reduction of terrestrial emission to space and cooling by reflection of incoming solar radiation. Quantification of the net effect is subject to errors in both longwave (LW) and shortwave (SW) radiative flux measurements, or in model calculations. The net radiative effect of high-level clouds depends on cloud height, optical thickness, areal fraction and cloud microphysical properties such as ice particle size and ice habits. Accurate representation of clouds, their radiative effects and associated climate feedbacks is one of the greatest challenges in climate model simulations and climate change predictions [*Cess et al.*, 1990, 1996; *Stephens*, 2005].

High-altitude clouds in the tropics include deep convective towers and associated anvil clouds, as well as thin cirrus that can be formed in situ by gravity wave and Kelvin wave perturbations or by large-scale uplift of humid layers [*Massie et al*. 2002]. The relationships of deep convection and associated clouds to sea surface temperature (SST) are of great interest in climate studies because of their importance for cumulus parameterizations in models and their potential implications for cloud feedbacks in climate change. A number of studies have been conducted using various measures of cloud observations and numerical models [e.g. *Graham and Barnett*, 1987; *Waliser et al*., 1993; *Ramanathan and Collins*, 1991, hereafter RC1991; *Lau et al.*, 1997; *Tompkins and Craig*, 1999; *Lindzen et al*., 2001, hereafter LCH2001; *Hartmann and Larson*,

2002; *Del Genio and Kovari*, 2002; *Bony et al*., 2004; *Lin et al*., 2006]. However, no consensus has been reached regarding whether high-altitude clouds increase or decrease with SST and whether they provide a positive or negative climate feedback. For example, RC1991 showed that the radiative forcing of cirrus anvils increases during El Niño; and the increase of their SW cooling effect is larger than the increase of their LW warming effect. They suggested that the optical thickness of cirrus anvils must increase when SST increases, in addition to the increase in the extent of cloudiness and the height of cloud top. They speculated that cirrus anvils may act like a "thermostat" to limit further warming of SST. This viewpoint has been challenged by a number of studies that highlighted the roles of evaporation, large-scale circulation, and ocean dynamics in regulating tropical SST [*Wallace*, 1992; *Fu et al*., 1992; *Hartmann and Michelsen*, 1993; *Pierrehumbert*, 1995; *Sun and Liu*, 1996].

Another viewpoint regarding the cirrus-SST relation and its climate feedback is the "iris hypothesis" proposed in LCH2001, in which cirrus anvil coverage averaged over the western Pacific was found to decrease with the cloud-weighted SST (CWT, defined as the average SST weighted by cloud fraction for the area 130ºE-170ºW, 30ºS-30ºN). The cloud data were based on the infrared brightness temperature (T_b of 11 and 12 μm channels) from the Japanese Geostationary Meteorological Satellite (GMS). In order to account for the impact of changing large-scale circulation and SST gradients on clouds [*Lindzen and Nigam*, 1987; *Hartmann and Michelsen*, 1993; *Lau et al*., 1997; *Bony et al*., 2004], LCH2001 postulated a normalization procedure in which cirrus anvil coverage was divided by the cumulus coverage. It attempted to deal with the varying detrainment from cumulus convection when SST changes rather than varying cumulus convection itself, which may be related to shifting patterns of large-scale circulation and SST gradients. Such an attempt is reasonable but the normalization would work

81 only if cirrus anvil coverage were proportional to the cumulus coverage. Without addressing the
82 pre-conditions for the normalization procedure, LCH2001 claimed that cirrus coverage normalized
83 by cumulus coverage decreases about 22% per degree increase of CWT, analogous to an eye's iris
84 when exposed to stronger light. They further inferred that the "iris" effect would produce a strong
85 negative climate feedback. There have been intense debates about the validity of the "iris
86 hypothesis" concerning the analysis approach and interpretation of the results [*Hartmann and*
87 *Michelsen*, 2002a, b, c (hereafter HM2002); *Lindzen et al*., 2002] as well as the assumptions of the
88 radiative properties of high clouds [*Fu et al*., 2002; *Lin et al*., 2002; *Chambers et al*., 2002; *Chou*
89 *et al*., 2002a, b]. In particular, HM2002 argued that the definition of CWT may automatically
90 produce a negative correlation of mean cloud fraction with CWT, provided that the variation of
91 cloud fraction over the cold waters is much greater than that over the warm waters. They showed
92 that the negative correlation of cirrus anvil fraction with CWT may arise from the large cloud
93 variations in the subtropics driven by meteorological forcing associated with mid-latitude storms.
94 Constraining the averaging domain to lower latitudes away from the subtropics may avoid the
95 definition problem of the CWT, but no reduction of anvil fraction relative to cumulus core fraction
96 was found in the analysis of HM2002. *Del Genio and Kovari* (2002) analyzed the Tropical
97 Rainfall Measuring Mission (TRMM) data and found that precipitation efficiency and cirrus
98 detrainment efficiency both increase with increasing SST, with the former increasing faster than
99 the latter. *Lin et al.* (2006) showed that the area coverage of tropical deep convective systems
100 increases with SST along with their precipitation efficiency. *Rapp et al*. [2005] examined the ratio
101 of deep convective cloud area to surface rainfall and found the ratio has no significant dependence
102 on underlying SST, except for warm rain processes, where the cloud area to rainfall ratio
103 decreases with SST, which may yield a positive feedback for reduced reflection of solar radiation.

104 However, these studies were based on cloud information derived from TRMM data, which may
105 underestimate thin cirrus clouds in the UT. A complete understanding of tropical high clouds and
106 their radiative impacts requires more accurate and comprehensive cloud datasets.

107 New satellite observations from the National Aeronautics and Space Administration (NASA)'s
108 "A-train" satellite constellation [*Schoeberl and Talabac*, 2006] provide new information on global
109 cloud variability. The A-train satellites are sun-synchronous, with equatorial crossing times around
110 1:30 am (descending orbits) and 1:30 pm (ascending orbits). The orbit tracks repeat every 16 days.
111 In particular, we use observations from the Atmospheric Infrared Sounder (AIRS) on the Aqua
112 satellite [*Parkinson*, 2003; *Chahine et al*., 2006]. It provides effective cloud fraction (CFR) and
113 cloud top pressure (CTP), along with temperature and moisture profiles, information on trace gas
114 species, and surface properties starting from September 2002. The Microwave Limb Sounder
115 (MLS) on the Aura satellite [*Schoeberl et al.*, 2006; *Waters et al*., 2006], for the first time,
116 provides the upper tropospheric (UT) ice water content (IWC) profile at 215 hPa and above,
117 starting from August 2004. The ice water path (IWP) can then be computed by the mass-weighted
118 vertical integration of IWC from 215 hPa to the cloud top heights. The AIRS and MLS
119 observations are only about 8 minutes apart [*Kahn et al*., 2007], and there are about 5-6 AIRS
120 measurements within each MLS field of view (FOV). CloudSat and CALIPSO are new members
121 of the A-train (launched in June 2006) that measure cloud liquid and ice water content profiles
122 throughout the troposphere [*Stephens et al*., 2002]. However, the CloudSat/CALIPSO data are not
123 used in this analysis.

124 In this study, we present a new observational analysis of the UT cloud variations with SST. We
125 analyze not only the UT cloud fraction (from AIRS), but also the IWC and IWP measurements
126 (from MLS), which are critical to determine the cloud radiative forcing. The improved precision

and coverage of these datasets compared to previous ones and especially the new vertically-stratified IWC information enable new investigations of the cloud and SST relations. We use UT clouds to refer to the high-altitude clouds observed by AIRS and MLS without distinction between different cloud types or sources of origin. Separation of deep convective cores, anvil clouds and thin cirrus will be explored in future work. In contrast to a recent study by *Su et al.* [2006a], which analyzed the spatial correlation of MLS IWC/IWP with SST on monthly and annual time scales, this paper focuses on the temporal variation of UT CFR and IWC/IWP on a daily time scale, as in LCH2001. We are interested in the total cloud changes averaged over the entire tropics. Zhang et al. (1996) showed that the relationship of cloud radiative forcing and SST varies from basin to basin, and the cloud and SST relationship for more limited regions differs from that averaged over the entire tropics. These differences are caused by variability in the large-scale atmospheric circulation that complicates the SST influence on convection and associated cloud changes. Using an average over the entire tropics does include compensatory cloud changes due to large-scale circulations, but avoids arbitrary boundary specifications and is more representative of changes in bulk cloud amount in response to the mean SST change. The observed relationships among these quantities can serve as useful references for global model simulations [e.g. *Su et al.* 2006b].

To facilitate the comparison with LCH2001, we use a similar analysis approach as used in their study: i.e., we examine the scatter plots of the UT CFR and IWC/IWP versus CWT and identify apparent relationships. We recognize the intrinsic problem of using the CWT definition as pointed out by HM2002. To deal with this problem, we have expanded the analysis into two parts. First, different tropical latitude belts are analyzed and compared. Second, the spatial patterns of UT CFR and IWC/IWP relations to CWT are examined so that the regional difference of cloud and SST relations are revealed. Moreover, the tropical-mean precipitation changes with CWT are

investigated simultaneously and compared to that of the UT CFR and IWP. We also use precipitation to normalize CFR or IWP by dividing the mean CFR or IWP by the mean precipitation in an analogous procedure to LCH2001 which used deep cumulus core fraction to normalize cirrus anvil fraction. The relationships of the precipitation-normalized CFR and IWP with the CWT are analyzed, the intricacies of the normalization procedure are addressed and the caveats of such a technique are noted.

The structure of the paper is as follows. Section 2 describes the datasets used for the analyses. Section 3 presents the UT clouds and SST relationships based on the AIRS and MLS observations. The UT cloud radiative effect and its changes associated with the IWC/IWP changes are discussed in Section 4. The conclusion and discussion are given in Section 5.

2. Data

We use AIRS Level 3 daily effective cloud fraction (CFR) and cloud top pressure (CTP) data on 1°×1° horizontal grids from September 1, 2002 to September 30, 2006 (version 4) [*Olsen et al*., 2005]. Both ascending (~1:30 pm local time) and descending (~1:30 am local time) orbits are included. Together they cover more than 90% of the globe, with each set of orbits alone covering about 80% of the globe (Figure 1). The AIRS CFR retrieval uses a radiance fitting procedure described in *Susskind et al*. [2003], with a horizontal resolution of ~15 km. To identify high-altitude clouds, we use the simultaneous AIRS Level 3 CTP measurement, which has a horizontal FOV of ~45 km in diameter, and has been validated against CloudSat, CALIPSO, and surface-based Atmospheric Radiation Measurement (ARM) observations [*Kahn et al*., 2007a, b]. Only grid boxes with CTP < 300 hPa are considered UT clouds. This value is chosen to match the MLS IWC measurement, which only goes down to 215 hPa. Early cross-comparison between the AIRS and MLS cloud measurements found that AIRS CTP tends to have a high pressure (i.e. low altitude)

173 bias compared to that derived from the MLS IWC measurements [*Kahn et al*., 2007a; *Wu et al*.,
174 2007]. We find that our results are not sensitive to the exact choices of CTP values between 450-
175 200 hPa. Throughout the remainder of this work, we use CFR to denote the UT cloud fraction with
176 CTP < 300 hPa. Note that the AIRS CFR represents a combined effect of cloud areal coverage and
177 cloud emissivity. For thick clouds, the emissivity is close to 1. Their CFR is thus approximately
178 fractional coverage. However, for thin clouds that are not opaque, the retrieved CFR is smaller
179 than the actual cloud coverage. Preliminary analysis indicates that the difference between the
180 AIRS retrieved CFR and the actual cloud coverage is about 0.2 (absolute difference) in the global
181 average [*Kahn et al*. 2007b]. Such caveats need to be considered when interpreting the results of
182 the analysis.

183 The Aura MLS Level 2 IWC measurements from August 8, 2004 to September 30, 2006
184 (version 1.5) are used. The IWC is retrieved from the cloud-induced radiance at 240 GHz [*Wu et*
185 *al*., 2006]. The v1.5 IWC is available at 215, 178, 147, 121, 100, 83 and 68 hPa, with a horizontal
186 resolution of 200-300 km along-track and ~7 km cross-track, and a vertical resolution of 3-4 km
187 [*Livesey et al*., 2005; *Wu et al*., 2006, 2007]. The Aura MLS IWC data have been validated against
188 in situ aircraft measurements and other satellite data [*Wu et al.*, 2007], and have been compared
189 with model simulations and analyses [*Li et al*., 2005]. The estimated IWC absolute accuracy is
190 within a factor of 2 and there may be *up to* 50% low bias compared to CloudSat IWC (version 4)
191 for single measurements, mostly for large IWC values due to instrument sensitivity [*Wu et al.*
192 2008]. On averages over large spatial domain and over periods longer than a few days, the
193 differences between MLS and CloudSat IWC are largely reduced [*Wu et al*. 2008]. The spatial
194 pattern of the MLS IWC resembles deep convective systems and associated anvil clouds [*Li et al*.,
195 2005; *Su et al*., 2006a]. The Level 2 data are obtained along MLS orbit tracks. The gap between

196 orbits is about 25° in the tropics (30ºS-30ºN) (Figure 1). The number of profiles each day is about
197 3500, with one-third of them within the tropics. Although the MLS daily data coverage is
198 relatively sparse, the daily cloud occurrence frequency in the tropical average is close to the MLS
199 monthly cloud occurrence frequency, suggesting that the tropical averages obtained from daily
200 data are adequately representative of the entire tropics. We note that both AIRS and MLS
201 measurements are only made up to twice per day for any given region and do not capture the full
202 diurnal cycles of tropical clouds. Since the daily mean values are of interest here, the impact of
203 diurnal variability is deferred to future study.
204

Insert Figure 1 here

205

206 We use the daily microwave SST product from the Advanced Microwave Scanning
207 Radiometer – EOS (AMSR-E) on the Aqua satellite (version 2) with a horizontal resolution of
208 0.25°×0.25°, processed at Remote Sensing Systems [*Donlon et al*., 2002]. To reduce sampling
209 errors, we average the AMSR-E SST to both AIRS and MLS data grids when performing
210 correlation analyses. The through-cloud capabilities of microwave radiometers reduce the
211 influence of clouds on the SST retrieval, and the daily coverage of the AMSR-E SST is an
212 improvement from the weekly SST product from the National Centers for Environmental
213 Prediction (NCEP) analysis, which was used in LCH2001.
214 We use the daily TRMM precipitation data (3B42) [*Huffman et al*., 2001] at a horizontal
215 resolution of 0.25°×0.25°. Averaging onto the AIRS and MLS data grids is performed for
216 coincident sampling, as for the AMSR-E SST.

217 **3. UT Clouds and SST Relations**

The daily mean UT cloud amount is defined as $\overline{A} = [\sum_n \cos\theta_n \cdot A_n] \Big/ \sum_n \cos\theta_n$, where A is either CFR, IWC or IWP, θ is the latitude, and n includes only oceanic measurements. For tropical mean SST, we use the cloud-weighted SST definition as in LCH2001, i.e., $CWT = [\sum_n CFR_n \cos\theta_n \cdot SST_n] \Big/ \sum_n CFR_n \cos\theta_n$. This reflects the importance of under-cloud SST as the forcing of cloud changes. We present the scatter plots of UT clouds versus the CWT for averages over 15ºS-15ºN. The results for averages over 30ºS to 30ºN and the area used in LCH2001 are summarized in Table 1 for comparison purpose. Besides the tropical mean cloud CFR, IWC and IWP relationship with the cloud-weighted SST, the spatial correlation of UT clouds with the cloud-weighted SST, and composite zonal means of UT clouds, precipitation and SST variations are also analyzed.

a. AIRS CFR-SST Relation

Figure 2a shows the AIRS tropical-mean UT cloud fraction ($\overline{CFR}$) scattered against the cloud-weighted SST for 15°S-15°N during the period of September 1, 2002 to September 30, 2006. Each dot corresponds to a daily average. All daily $\overline{CFR}$ occurs over the CWT greater than 300 K, indicating the close connection of AIRS observed UT clouds to tropical deep convection [e.g. *Graham and Barnett*, 1987; *Waliser et al*., 1993; *Su et al*., 2006a]. The daily $\overline{CFR}$ is quite scattered with respect to the CWT, but a positive slope is discernible, about 1.6 CFR% K^{-1} (~13% K^{-1} relative to the 4-year mean CFR of 12%). The correlation coefficient is about 0.2, rejecting the null hypothesis of zero correlation at the 95% significance level based on the Student's t-test. If we extend the area to 30ºS-30ºN, the regression slope reduces to 0.5 CFR% K^{-1} (~6% K^{-1} relative to the 4-year mean CFR), with a correlation coefficient of 0.16 (Table 1). If we perform the averaging over the western Pacific from 130ºE to 170ºW (30ºS-30ºN) as in LCH2001, the slope of

240 CFR versus SST is 0.8 CFR% K^{-1}, or 6% K^{-1} relative to its 4-year mean, with a correlation
241 coefficient of 0.12 (Table 1). The smaller regression slope of CFR versus the CWT for areas
242 including the subtropics indicates that the weaker SST influence away from the deep convective
243 regions. However, the correlation coefficients between the mean cloud fraction and the CWT are
244 generally weak in all regions examined, with the values even smaller than those in HM2002 using
245 the original datasets as LCH2001. Furthermore, the sign is reversed here.

246 The positive correlation of AIRS CFR with the CWT is different from the negative correlation
247 of anvil cloud coverage with the CWT as shown in LCH2001. This may be because the AIRS
248 CFR includes deep convective towers, anvil clouds and even thin cirrus while LCH2001 separated
249 anvil clouds from cumulus turrets. Second, the emissivity factor in the AIRS CFR may cause
250 biases in the CFR and CWT relation. Moreover, our dataset covers different periods from
251 LCH2001 and interannual variability may play a role in the different relations of UT cloud
252 fraction versus SST. Using the first two years and last two years of daily CFR regressed with the
253 corresponding CWT gives a positive slope of 1.1 and 1.9 CFR% K^{-1} (9% K^{-1} and 16% K^{-1}
254 relatively), respectively. Despite the difference in the magnitudes for different years, the AIRS
255 CFR appears to increase with the CWT.

256

Insert Figure 2 here

257

258 To examine the spatial distribution of the CFR relation to the CWT, we follow the analysis
259 techniques used in HM2002 to regress the time series of CFR at each 1°x1° grid onto the time
260 series of CWT (averaged over 30°S-30°N). The regressions are performed using both the original
261 unfiltered data and high-passed data, in which a 91-day running mean is removed to filter out the
262 low-frequency variability. We find the spatial patterns of regression coefficients are similar using

263 the unfiltered or high-passed data as in HM2002. Figure 3 shows the regression coefficients of
264 CFR on the CWT which has been high-pass filtered and divided by its standard deviation.
265 Consistent with HM2002, the regression coefficients of CFR on the CWT exhibit spatial
266 differences in deep tropics and subtropics; but to a much less extent than that in HM2002. The
267 regression coefficients are positive in climatologically convective regions and negative in non-
268 convective regions, with minima in the subtropical North Pacific and the southern Indian Ocean.
269 As HM2002 pointed out, negative regression of CFR with CWT tends to occur over cold waters.
270 However, we note that the magnitudes of regression coefficients in Fig. 3 are mostly within ±0.05
271 per standard deviation change of the CWT, much smaller than the values in HM2002 for cirrus
272 anvil fraction (based on T_b < 260 K) regressed on the CWT. This may be due to the different
273 datasets used. The UT cloud fraction derived from AIRS data includes deep convective cores and
274 thin cirrus generated from convective detrainment and in situ formation [e.g., *Boehm and Verlinde*
275 2000]. They appear to be less sensitive to the underlying SST change than the anvil fraction based
276 on T_b < 260 K in HM2002.
277
Insert Figure 3 here
278
279 LCH2001 hypothesized that increasing precipitation efficiency with increasing surface
280 temperature may reduce the cirrus outflow. We analyzed the TRMM precipitation dataset and
281 examined its variation with SST and CFR. Figure 2b shows the scatter plot of the $\overline{CFR}$ versus
282 the mean precipitation ($\overline{P}$) for 15°S-15°N. The correlation coefficient between $\overline{CFR}$ and $\overline{P}$ is
283 0.55, statistically significant above the 95% level. When $\overline{P}$ is scattered against the CWT, a
284 positive correlation of 0.2 is found (Fig. 2c). The $\overline{P}$ increases with the CWT at a rate of 0.2 mm
285 day^{-1} K^{-1}, about 16% K^{-1} relative to its 4-year mean. When we define a precipitation-

normalized CFR by simply dividing $\overline{CFR}$ by $\overline{P}$ and scatter the ratio of cloud fraction to precipitation against the CWT, we find the precipitation-normalized cloud fraction appears to be insensitive to SST changes, with a slightly negative slope of −0.2 CFR% mm^{-1} day K^{-1} (Fig. 2d), corresponding to −2% K^{-1} relative to the 4-year mean. The correlation coefficient between the precipitation-normalized cloud fraction and the CWT is only −0.02, suggesting virtually no linear correlation.

However, a caveat needs to be pointed out regarding this normalization procedure, which is analogous to the normalization of cirrus anvil fraction by deep convective core fraction used in LCH2001. As shown in Fig. 2b, tropical-mean cloud fraction is not simply proportional to the tropical-mean precipitation, since the linear regression line has a non-zero intercept. Thus, simply dividing cloud fraction by precipitation would result in a term inversely proportional to the mean precipitation in addition to the regression slope of cloud fraction to precipitation, and only the latter is the quantity of relevance to the detrainment of cirrus clouds per unit convection. Hence, although the normalization is appealing, simply dividing the cloud fraction by precipitation does not provide a good solution to isolate the cirrus detrainment change from the cumulus convection change itself. Given the non-proportionality between cloud fraction and precipitation, we are inclined to be cautious about inferring cirrus detrainment change using this normalization procedure.

For the entire tropics within 30ºS-30ºN, the precipitation-normalized CFR also shows a slightly negative regression slope with the CWT, about −1% K^{-1} (Table 1), but the correlation coefficient is close to zero. For the region analyzed in LCH2001, the slope of the precipitation-normalized CFR versus SST is only 0.1% K^{-1}, an almost flat regression line. Considering that the AIRS CFR convolves emissivity and areal coverage, the actual cirrus areal coverage is

309 substantially higher than the CFR, especially for thin cirrus [*Kahn et al.* 2007b]. This may yield
310 a somewhat stronger negative slope in Fig. 2d if warmer SST is associated with thicker UT
311 clouds.
312
Insert Figure 4 here
313
314 Figure 4 further illustrates the relations among SST, cloud fraction and precipitation in terms
315 of zonal averages. It shows the composite zonal mean SST, CFR and precipitation for days when
316 CWT was lower than the 4-year average (solid lines, the "lower SST days") and vice versa
317 (dashed lines, the "higher SST days") using both unfiltered (Fig. 4a) and high-passed (91-day
318 running mean removed, Fig. 4b) data. Although this composite procedure was similar to
319 HM2002, the results we obtain bear different characteristics from HM2002 (their Fig. 5), mainly
320 because different datasets are analyzed here, which may be associated with different cloud
321 systems. In HM2002, the anti-correlation of CWT with anvil cloud fraction primarily resulted
322 from the cloud fraction variations in latitudes greater than 15º. The equatorial anvil cloud
323 fraction changes were smaller than those in the subtropics. In our composites (Fig. 4), the CWT
324 seems in phase with the northern hemispheric SST and out of phase with the southern
325 hemisphere SST, arising from the seasonal shifts of SST patterns. Since the cloud fraction in the
326 northern hemisphere is larger on average than that in the southern hemisphere, the CWT
327 variation is dominated by the northern hemispheric SST. Noticeable differences in cloud fraction
328 between the "lower SST days" and the "higher SST days" are found through all tropical
329 latitudes, which are positively correlated with each hemispheric zonal SST changes. Similarly,
330 zonal precipitation changes follow the zonal SST changes. Figure 4b shows the zonal-mean
331 SST, CFR and precipitation variations when seasonal cycles are removed. Again, we find CFR

and precipitation changes positively correlate with SST changes for most tropical latitudes. Large changes of CFR and precipitation are within 10ºS-10ºN. Outside 10ºS-10ºN, the changes of CFR and precipitation are quite small.

In summary, the tropical-mean UT cloud fraction has a weakly positive correlation with the underlying SST. We do not observe a negative correlation of the UT CFR with the CWT as in LCH2001. Comparing to the precipitation increase with the CWT, the UT cloud fraction increases at a similar rate. No distinct correlation is found between the CWT and the ratio of the UT CFR to the precipitation.

On the other hand, CFR is only one measure of UT cloud amount. Cloud optical depth, which is dependent on IWC and cloud height, is a more radiatively relevant cloud quantity. The changes of IWC with SST can alter the net radiative forcing of the UT clouds in addition to that caused by the cloud fraction changes. Therefore, we have analyzed the IWC measurements from MLS to better quantify the UT cloud variations with SST.

Insert Figure 5 here

b. MLS IWC-SST Relation

Figure 5 shows the daily tropical-mean MLS IWC scattered against the CWT for 15°S-15°N during the period from August 8, 2004 to September 30, 2006. The definition of $\overline{IWC}$ is similar to $\overline{CFR}$. For each day, the CWT is computed using the AMSR-E SST weighted by the AIRS CFR, both sampled onto the MLS IWC measurement location. Three vertical levels of IWC are shown in Figure 5, 100 hPa (~16 km), 147 hPa (~13.5 km) and 215 hPa (~11 km). All exhibit an increase of $\overline{IWC}$ with increasing CWT, albeit with a large scatter. The rates of the $\overline{IWC}$ increase with the CWT are 0.3 mg m^{-3} K^{-1} at 215 hPa, 0.2 mg m^{-3} K^{-1} at 147 hPa and 0.03 mg m^{-3} K^{-1} at 100 hPa.

354 The percentage changes relative to the 2-year mean at each level are approximately 15% K^{-1} at
355 215 hPa, 34% K^{-1} at 147 hPa, and 60% K^{-1} at 100 hPa. The correlation coefficients between the
356 IWC and the CWT are 0.2 at 215 hPa, 0.3 at 147 hPa and 0.2 at 100 hPa, all statistically
357 significant above the 95% level.

358

Insert Figure 6 here

359

360 Figure 6 shows the scatter plot of the vertically-integrated IWC, i.e., IWP, versus the CWT,
361 and the scatter plots of IWP versus precipitation and the precipitation-normalized IWP versus the
362 CWT. The rate of the increase of the $\overline{IWP}$ with the CWT is 1.4 g m^{-2} K^{-1}, about 26% K^{-1} relative
363 to the 2-year mean IWP. The correlation coefficient between $\overline{IWP}$ and the CWT is about 0.3. The
364 tropical-mean precipitation $\overline{P}$ is positively correlated with $\overline{IWP}$ with a correlation coefficient of
365 0.6. However, we note that $\overline{IWP}$ and $\overline{P}$ are not strictly proportional, indicated by the two different
366 slopes for the least-squares fitted line and the line constrained to go through zero (Fig. 6b). Thus
367 the relation of the precipitation-normalized IWP with SST (Fig. 6c) does not completely remove
368 the precipitation dependence on SST, similar to the precipitation-normalized CFR shown in Fig.
369 2d. Despite the fact that the term inversely proportionally to precipitation would yield a negative
370 tendency for the precipitation-normalized IWP relation with SST, the precipitation-normalized
371 IWP exhibits a positive slope with the CWT, at the rate about 15% K^{-1}, with a correlation
372 coefficient of 0.2. Similar results are found for 30°S-30°N and the region used in LCH2001 (Table
373 1). The increase of $\overline{IWP}$ with the CWT occurs at a greater rate than that of precipitation for all
374 three areas analyzed.

Insert Table 1 here

375

376 The composite zonal averages of SST, IWP and precipitation are shown in Fig. 7 for the days
377 when the CWT is higher (dashed lines) or lower (solid lines) than the 2-year mean. Compared to
378 the zonal means in Fig. 4 based on the 4-year 1°x1° gridded data, the zonal averages constructed
379 from the 2-year data on the MLS tracks appear noisier. The high-passed (91-day running mean
380 removed) zonal-mean SST (Fig. 7b, top panel) shows little difference (~0.02 K) between the
381 "higher SST days" and the "lower SST days" for the two years. Nevertheless, both the unfiltered
382 and high-passed data show that the higher CWT is associated with larger IWP for most of tropical
383 latitudes. The precipitation tracks the SST latitudinal variation quite well, even though the high-
384 passed precipitation is very noisy. Similar to Fig. 4b, it is not obvious that the subtropical cloud
385 variations are greater than that in the deep tropics, different from the results shown in HM2002.

386 **Insert Figure 7 here**

387 **4. Exploring the radiative effect of UT clouds**

388 The motivation to examine the UT cloud fraction and IWC changes with SST resides in the
389 importance of the radiative forcing of these clouds to the Earth-atmosphere climate system. It is
390 useful to estimate how much the cloud radiative effect may change given the rate of UT cloud
391 changes with SST. However, a limitation of our datasets is the lack of cloud profiles below 215
392 hPa. Thus an accurate quantification of the total cloud radiative forcing is not possible with only
393 the datasets used in this study. Nevertheless, we carry out some calculations to obtain a qualitative
394 estimate of the radiative effect of the UT clouds and the sensitivity of the cloud radiative effect to
395 UT cloud changes. Our calculations are focused on the tropical-mean cloud forcings. These
396 calculations are considered to be idealized but they help to shed light on understanding the cloud
397 feedback problem.

398 The radiative transfer model we use is the Fu-Liou radiation model. It uses the delta-four-
399 stream approximation for solar flux calculations [*Liou et al*., 1988] and delta-two-stream
400 approximation for infrared flux calculations [*Fu et al*., 1997]. The incorporation of non-grey
401 gaseous absorption in multiple-scattering atmospheres is based on the correlated *k*-distribution
402 method developed by *Fu and Liou* [1992]. The solar and infrared spectra are divided into 6 and 12
403 bands, respectively, according to the location of absorption bands. Parameterization of the single-
404 scattering properties for ice cloud follows the procedure developed by *Fu and Liou* [1993]. The
405 spectral extinction coefficient, the single-scattering albedo, and the asymmetry factor are
406 parameterized in terms of the IWC and the effective ice crystal size (D_e). For D_e, instead of using
407 the mono-distribution as in the standard Fu-Liou code, we adopt the empirical formula for ice
408 particle size distribution developed by *McFarquhar and Heymsfield* [1997] (the MH distribution)
409 as used in the MLS IWC forward model, where D_e is computed as a function of MLS measured
410 IWC and temperature. This treatment of ice particle size is consistent with the MLS IWC retrieval
411 and is considered to be an improvement over other more arbitrary assumptions of ice particle size.
412 We perform the radiation calculations for two cases. In one case, we treat all MLS observed
413 UT clouds as "single-layer' clouds, with no clouds underneath (the "single-layer" case). This
414 treatment has been a common practice in isolation of the radiative effect of certain types of clouds
415 [e.g. *Fu and Liou*, 1993; *Hartmann et al.*, 2001; *Fu et al.,* 2002]. Another case takes into account
416 the influence of lower clouds by using the tropical climatological values for both the low and
417 middle-altitude clouds from the International Satellite Cloud Climatology Project (ISCCP)
418 [*Rossow and Schiffer*, 1991] below the AIRS and MLS observed UT clouds, with random
419 overlapping in the vertical (the "multi-layer" case). The UT cloud radiative effect (CRE) is thus the
420 difference of LW and SW fluxes at the top of atmosphere (TOA) with and without the observed

421 UT clouds while other conditions (surface, atmospheric profiles and low and middle-altitude
422 clouds) are held the same.

423 Because of the non-linearity of cloud radiation calculations, it is necessary to compute the
424 radiative fluxes using instantaneous UT cloud profiles along orbit tracks, rather than using
425 averaged profiles over a certain area or period. The monthly tropical-mean CRE is then
426 constructed by averaging all individual CREs, totalling about 35000 calculations per month within
427 the tropics (30°S-30°N). For both clear-sky and all-sky radiative flux calculations, the standard
428 tropical atmospheric profile is used instead of the observed atmospheric profiles such as those from
429 AIRS. Using a uniform atmospheric profile isolates the cloud forcing due to cloud properties alone
430 rather than the convoluted effects from clouds and associated temperature and water vapor changes
431 [*Soden et al*., 2004]. In the tropical-mean, the difference of CREs from using the standard
432 atmospheric profile or spatially-varying observed profiles should be quite small.

433 We consider that each MLS measurement footprint has fractional cloud coverage η, determined
434 by the AIRS UT cloud fraction interpolated on the MLS FOV. Since the MLS measurements
435 represent the averaged IWC over the MLS FOV, the actual overcast IWC value is IWC/η. We test
436 the sensitivity of CRE to the estimate of η by augmenting AIRS CFR by 0.2 (the "+0.2 CFR run")
437 or assuming that the UT cloud coverage for each MLS IWC FOV is 100% and the AIRS CFR
438 equals the cloud emissivity (the "overcast run").

439

Insert Table 2 here

440

441 Using January 2005 as an example, Table 2 lists the calculated monthly tropical-mean UT
442 cloud forcing for different radiation model runs. In the "single layer" case, assuming η = AIRS
443 CFR, the net UT cloud CRE is about 2.7 W m^{-2} (warming) in the tropical average, with LW CRE

444 being 4.7 W m^{-2} and SW CRE being −2.0 W m^{-2}. Increasing η by 0.2 would increase the LW and
445 SW CREs by 0.3 and 0.03 W m^{-2} in magnitude, respectively, resulting in 3.0 W m^{-2} warming in
446 the tropical average. The "overcast" run yields a significantly larger LW warming effect. The
447 tropical-averaged net CRE becomes 17.6 W m^{-2}, with 21.4 W m^{-2} LW CRE and −3.8 W m^{-2} SW
448 CRE.

449 In the "multi-layer" case, we use the low and middle cloud climatology taken from *Dessler et*
450 *al.* [1996], which were based on the ISCCP data for February-March 1984 to 1988, averaged over
451 0º−10ºS. The low clouds are specified from 855 hPa to 760 hPa, with a visible optical depth of 20
452 and a fraction of 19%. The middle-altitude clouds are specified from 525 hPa to 462 hPa, with a
453 visible optical depth of 10 and a fraction of 16%. Both have an emissivity of 1. The cloud effective
454 radii are 11 μm for middle clouds and 10 μm for low clouds [*Dessler et al*., 1996]. The UT cloud
455 fractional coverage η is based on the AIRS CFR interpolated onto the MLS IWC measurement
456 location. Under the random overlapping assumption, we obtain a tropical mean OLR of 268 W m^{-2},
457 and a tropical reflectivity of 0.3. Compared to the Earth Radiation Budget Experiment (ERBE)
458 tropical climatology [*Barkstrom*, 1984], the OLR is overestimated by 5% and the reflectivity is
459 overestimated by about 30%. The Clouds and the Earth's Radiant Energy System (CERES) tropical
460 climatology gives a slightly higher OLR and reflectivity than ERBE and the errors of our estimates
461 relative to CERES are still close to 30% for SW fluxes. However, because the UT cloud forcing is
462 of interest, we focus our attention on the differences of TOA LW and SW fluxes with and without
463 UT clouds. In the "multi-layer" case, the LW CRE of the UT cloud is smaller than the "single-
464 layer" case by 0.4 W m^{-2} in the tropical average as the low and middle clouds reduce the terrestrial
465 emission reaching the upper levels. The SW CRE also decreases to −1.5 W m^{-2}, resulting in a net

466 CRE of 2.8 W m^{-2}, close to the "single-layer" case (Table 2). Varying the low and middle cloud
467 optical properties moderately does not change the magnitude of UT CRE significantly.

468 Our estimates of the net UT cloud forcing are consistent with previous results of high cloud
469 forcing calculated from models or obtained from observations. *Hartmann et al.* [1992] regressed
470 the ERBE radiative flux data on the ISCCP cloud data to investigate the radiation effect of each
471 cloud type. They found that high thin cloud (optical depth less than 9.38, cloud top < 440 hPa)
472 produced a net warming of 2.3 W m^{-2} in DJF in the global-average. *Chen et al.* [2000] calculated
473 the radiative effect of each ISCCP cloud type in a radiative transfer model and showed that cirrus
474 cloud (optical depth < 3.6, cloud top < 440 hPa) has a net warming of 1.3 W m^{-2} at TOA in the
475 global average. For "overcast" high clouds, the model calculations by *Hartmann et al.* [2001] and
476 *Fu et al.* [2002] suggested that high clouds with cloud top pressure less than 300 hPa and optical
477 depth less than 4 have a net warming effect around 20 W m^{-2}. When multiplied by their fractional
478 coverage, the net high cloud forcing is on the order of a few W m^{-2}. As 99% of the MLS observed
479 ice clouds have optical depth less than 4, they fall into the category of high thin clouds or cirrus by
480 the ISCCP definition. Our calculated UT CREs are within the range of previous theoretical or
481 observational estimates, especially for tropical-means. Qualitatively, these UT clouds alone would
482 produce a net warming at TOA.

483 **Insert Figure 8 here**

484

485 Since the UT IWC tends to increase with SST more than does the cloud fraction, we conduct a
486 set of sensitivity runs to investigate the change of CRE due to the changes of IWC. We
487 successively increase the IWC values at each height uniformly over the tropics by 25% to 250%,
488 while keeping cloud fraction unchanged. For simplicity, the "single-layer" approach is used. Based
489 on the previous calculations, the results obtained from the "single-layer" case is applicable to the

490 "multi-layer" case, in terms of the sign and approximate magnitude of UT CRE. Figure 8 shows
491 that the tropical-mean net warming reaches its maximum when IWC is increased by 25%-50%
492 from the current value. When IWP is increased by 50%, The net warming is 0.05 W m^{-2} more than
493 the standard run, with LW and SW effects both increasing by 0.7 W m^{-2}. Supposing the rate of
494 IWC increase with SST is about 26% K^{-1} as shown in Fig. 5a and Table 1, the change of net CRE
495 with SST is about 0.02 W m^{-1} K^{-1}, while the separate changes of LW and SW CRE are larger.
496 When IWC is increased more than 50%, the increase in SW cooling outweighs LW warming,
497 causing the net CRE to decrease from its maximum value. When IWC is increased by 75%, the net
498 CRE returns to approximately the same value as the standard run, although the changes in the LW
499 and SW effects are both about 1.0 W m^{-2} in the tropical average. A further increase of IWC yields
500 net warming smaller than the standard run, although it is unlikely the polarity of the net CRE
501 would reverse sign given reasonable IWC changes for hypothetical SST changes up to a few
502 degrees. These UT clouds would provide a persistent warming effect even when their IWC is more
503 than doubled. Note that these sensitivity runs also provide an estimate of UT cloud forcing errors
504 when the bias in MLS IWC measurements is considered. The doubled IWC run gives an upper
505 bound of cloud forcing uncertainty (< 0.05 W m^{-2}) due to the low bias in IWC single
506 measurements. If all MLS IWC measurements were 50% lower than the actual IWC, further
507 increase of UT IWC would tend to reduce the net warming and correspond to a negative cloud
508 feedback. However, since the tropical-mean MLS IWC is not significantly lower than that of
509 CloudSat, our estimate of tropical-mean UT CRE is useful in a reasonable range.

510 **5. Conclusion and discussion**

511 Two aspects of tropical upper tropospheric cloud variations with SST are analyzed using new
512 cloud observations from AIRS and MLS. One aspect is UT cloud area fraction (CFR) and the

513 other is ice water content (IWC), which is directly linked to cloud optical thickness. Averages of
514 cloud quantities and precipitation over tropical oceans are scattered against the cloud-weighted
515 SST (CWT) and their relationships with the CWT are identified. Daily tropical-mean UT cloud
516 fraction from AIRS tends to increase with the CWT, at a comparable rate to the tropical-mean
517 precipitation increase with the CWT, close to 15% K^{-1} for 15ºS-15ºN and 5% K^{-1} for 30ºS-30ºN.
518 Measures of UT cloud ice, IWC and IWP, are found to increase with the CWT at a rate ~26% K^{-1}
519 for 15ºS-15ºN and ~16% K^{-1} for 30ºS-30ºN, faster than does the tropical-mean precipitation. The
520 reduced rates of increase with the CWT when more subtropical areas are included in averaging
521 may suggest the influence of mid-latitude storms [*HM2002*]. Examination of the zonal-averages of
522 SST, CFR, IWP and precipitation shows that the positive correlations of CFR and IWP with the
523 CWT occur universally over the deep tropics within 10-15 degrees from the equator. Further away
524 from the equator into the subtropics, dynamical effects not related to SST may contaminate the
525 CFR and IWP relations with the CWT. However, we do not find greater CFR or IWP changes near
526 the subtropics than in the deep tropics as in HM2002. Instead, the AIRS CFR and MLS IWP show
527 relatively large changes within the deep tropics.

528 We also adopt a procedure as in LCH2001 which normalizes CFR or IWP by precipitation and
529 regress the ratio with the CWT. Although the intent of normalizing cloud statistics by a measure
530 related to convective mass flux is appealing [*LCH2001*], we show that such a normalization
531 procedure that assumes proportionality appears to face inherent problems. For the data considered
532 here, proportionality does not hold between precipitation and CFR or IWP. While the
533 normalization procedure thus does not appear to be a reliable means of taking out the effects of
534 large-scale circulations and SST gradients, and we do not recommend it for inference regarding
535 climate change, we nonetheless examine the results of this procedure, and do not find a significant

536 negative relationship with CWT. However, the observed variations of UT CFR, IWC, IWP and
537 precipitation with the CWT provide useful reference values for evaluation of cloud simulations in
538 climate models.

539 The radiative effect of the UT clouds observed by AIRS and MLS is estimated using the Fu-
540 Liou radiative transfer model. We emphasize the qualitative aspect of the radiation calculations
541 due to uncertainties associated with missing low and middle level clouds, the estimate of cloud
542 fraction and other factors. We find that UT clouds have a dominant infrared-warming effect owing
543 to their small visible optical depth, consistent with previous studies. Increasing the UT IWC by
544 50% would increase the net cloud forcing by about 0.05 W m^{-2}, corresponding to a small positive
545 feedback and a sensitivity to SST around 0.02 W m^{-2} K^{-1}. However, the small change in net CRE
546 is associated with relatively large changes in LW and SW fluxes separately, which can have a non-
547 negligible effect on atmospheric heating rate and surface energy budget. Further increases of IWC
548 would reduce the magnitude of net warming due to the nonlinearity in the net CRE with IWC.
549 However, for any reasonable increase of tropical mean SST (within a few degrees), the net
550 radiative forcing of these UT clouds remains positive (warming). Measurement uncertainties in UT
551 CFR and IWC greatly affect the magnitude of cloud forcing but the qualitative change of cloud
552 radiative effects holds for a reasonable range.

553 We note that our analysis focuses on the upper-most clouds in the troposphere. We do not find
554 a negative correlation of the UT cloud fraction with the underlying SST. The variations of the UT
555 clouds with SST are consistent with increases in tropical deep convection with SST, with the
556 caveat that this is in part associated with changes in SST gradients for the variability observed
557 here. The implication that stronger convection produces thicker cirriform clouds when local SST
558 increases qualitatively agrees with RC1991, although the radiative effect of UT clouds derived

559 here is different from the cloud forcing in RC1991, which included the deep convective clouds and
560 anvils in the whole tropospheric column. With the emerging new tropospheric cloud profiles from
561 CloudSat/CALIPSO, we are hopeful that a better understanding of tropical cloud variability and a
562 more accurate quantification of cloud radiative impact can be attained.
563
564 **Acknowledgments.** We thank MLS and AIRS colleagues for data support. Discussions with A.
565 Dessler, Q. Fu, B. Lin, R. S. Lindzen, and R. Rondanelli were helpful. This work was carried out
566 at the Jet Propulsion Laboratory, California Institute of Technology, under contract with NASA.
567 JDN is supported by National Science Foundation Grant ATM-0645200 and NOAA Grant
568 NA05OAR4311134. We thank three anonymous reviewers for helpful comments and suggestions.

References

Ackerman, S., K. Strabala, P. Menzel, R. Frey, C. Moeller, B. Gumley, B. Baum, S. W. Seeman, and H. Zhang, 2002: Discriminating clear-sky from cloud with MODIS-algorithm theoretical basis document (MOD35), in *MODIS Algorithm Theoretical Basis Document*, NASA.

Barkstrom, B. R., 1984: The Earth Radiation Budget Experiment (ERBE), *Bull. Am. Meteorol. Soc. 65*, 1170-1185.

Betts, A. K., Greenhouse warming and the tropical water budget, *Bull. Am. Meteorol. Soc. 71*, 1464-1465, 1990.

Boehm, M. T., J. Verlinde, 1990: Stratospheric influence on upper tropospheric tropical cirrus, Geophys. Res. Lett., 27(19), 3209-3212, 10.1029/2000GL011678.

Bony, S., J.-L. Dufresne, H. LeTreut, J.-J. Morcrette, and C. Senior, 2004: On dynamic and thermodynamic components of cloud changes. *Climate Dyn*., **22**, 71-86.

Cess R. D., Coauthors, 1990: Intercomparison and interpretation of climate feedback processes in 19 atmospheric GCMs. *J. Geophys. Res.*, **95**, 16601–16615.

Cess R. D., Coauthors, 1996: Cloud feedback in atmospheric general circulation models: An update. *J. Geophys. Res.*, **101**, 12791–12794.

Cess, R. D.; Zhang, M.; Wielicki, B. A.; Young, D. F.; Zhoou, X-L.; Nikitenko, Y., 2001: The influence of the 1998 El Nino upon cloud-radiative forcing over the Pacific warm pool, *J. Climate*, 14, 2129-2137.

Chahine M. T, T. S. Pagano, H. H. Aumann, R. Atlas, C. Barnet, et al. (2006) AIRS: Improving Weather Forecasting and Providing New Data on Greenhouse Gases. *Bull. Am. Meteorol. Soc.*: Vol. 87, No. 7 pp. 911–926.

591 Chambers L., B. Lin, and D. Young, 2002: New CERES data examined for evidence of tropical
592 iris feedback. *J. Clim.*, **15**, 3719–3726.
593 Chen, T., W.B. Rossow, and Y. Zhang, 2000: Radiative Effects of Cloud-Type Variations. *J.*
594 *Climate*, 13, 264–286.
595 Chou, M.-D., R. S. Lindzen, and A.Y. Hou, 2002a: Reply to: "Tropical cirrus and water vapor: an
596 effective Earth infrared iris feedback?" *Atmospheric Chemistry and Physics*, **2**, 99-101.
597 Chou, M.-D., R. S. Lindzen, and A.Y. Hou, 2002b: Comments on "The Iris hypothesis: A negative
598 or positive cloud feedback?" *J. Climate*, **15**, 2713-2715.
599 Del Genio A. D., and W. Kovari. 2002: Climatic properties of tropical precipitating convection
600 under varying environmental conditions. *J. Clim*. 15, 2597-2615.
601 Dessler, A.E., K. Minschwaner, E.M. Weinstock, E.J. Hintsa, J.G. Anderson, and J.M. Russell, III,
602 The effects of tropical cirrus clouds on the abundance of lower stratospheric ozone, *J. Atmos.*
603 *Chem*., 23, 209-220, 1996.
604 Donlon, C. J., P. Minnett, C. Gentemann, T. J. Nightingale, I. J. Barton, B. Ward and, J. Murray,
605 2002: Towards Improved Validation of Satellite Sea Surface Skin Temperature Measurements
606 for Climate Research, *J. Clim,* **15**, No. 4, 353-369.
607 Fu, R., A. D. Del Genio, W. B. Rossow, and W. T. Liu, Cirrus-cloud thermostat for tropical sea
608 surface temperatures tested using satellite data, *Nature*, 358, 394-397, 1992.
609 Fu, Q., and K.N. Liou, 1992: On the correlated k-distribution method for radiative transfer in
610 nonhomogeneous atmospheres. *J. Atmos. Sci.*, 49, 2139-2156.
611 Fu, Q., and K. N. Liou, 1993: Parameterization of the radiative properties of cirrus clouds. *J.*
612 *Atmos. Sci.,* 50, 2008-2025.

613 Fu, Q., K.N. Liou, M. Cribb, T.P. Charlock, and A. Grossman, 1997: Multiple scattering in
614 thermal infrared radiative transfer. *J. Atmos. Sci.*, 54, 2799-2812.
615 Fu, Q., 1996: An accurate parameterization of the solar radiative properties of cirrus clouds for
616 climate models. *J. Climate*, 9, 2058-2082.
617 Fu, Q., M. Baker, D. L. Hartmann, 2002: Tropical cirrus and water vapor: An effective earth
618 infrared iris feedback? *Atmos. Chem. Phys*., 2, 1-7.
619 Gao, B. C., P. Yang, W. Han, R. R. Li, and W. J. Wiscombe, 2002: An algorithm using visible and
620 1.38 μm channels to retrieve cirrus reflectances from aircraft and satellite data, *IEEE Trans.*
621 *Geosci. Remote Sens.*, *40*, 1659–1668.
622 Graham, N. E. and T. P. Barnett, Sea surface temperature, surface wind divergence, and
623 convection over tropical oceans. *Science, 238,* 657-659,1987.
624 Hartmann, D.L., L. Moy, and Q. Fu, 2001: Tropical convection and the energy balance at the top
625 of the atmosphere. *J. Climate,* 15, 4495-4511.
626 Hartmann, D.L., M.E. Ockert-Bell, and M.L. Michelsen, 1992: The Effect of Cloud Type on
627 Earth's Energy Balance: Global Analysis. *J. Climate*, 5, 1281–1304.
628 Hartmann, D.L., and M.L. Michelsen, 1993: Large-scale effects on regulation of tropical sea
629 surface temperature. *J. Clim., 6,* 2049-2062.
630 Hartmann, D. L. and K. Larson, An Important Constraint on Tropical Cloud-Climate Feedback.
631 *Geophys. Res. Lett.*, *29*(20), 1951-1954, 2002.
632 Hartmann D. L., and M. L. Michelsen, No evidence for iris. *Bull. Amer. Meteor. Soc*., 83, 249-254,
633 2002a.
634 Hartmann, D.L., and M.L. Michelsen, Reply to the comments on “No evidence for iris”, *Bul.*
635 *Amer. Meteor. Soc*., 83, 1349-1352, 2002b.

636 Hartmann, D.L., and M.L. Michelsen, A two-box model of cloud-weighted sea surface
637 temperature: The semiautomatic negative correlation with mean cloud fraction, *Bul. Amer.*
638 *Meteor. Soc*., 83, 1352-1352, 2002c.
639 Huffman, G. J., R.F. Adler, M. Morrissey, D.T. Bolvin, S. Curtis, R. Joyce, B McGavock, J.
640 Susskind, 2001: Global Precipitation at One-Degree Daily Resolution from Multi-Satellite
641 Observations. J. Hydrometeor., 2(1), 36-50.
642 Kahn, B.H., A. Eldering, A.J. Braverman, E.J. Fetzer, J.H. Jiang, E. Fishbein, and D.L. Wu, 2007:
643 Towards the characterization of upper tropospheric clouds using Atmospheric Infrared Sounder
644 and Microwave Limb Sounder observations, *J. Geophys. Res. 112*, D05202,
645 doi:10.1029/2006JD007336.
646 Kahn, B. H., Chahine, M. T., Stephens, G. L., Mace, G. G., Marchand, R. T., Wang, Z., Barnet, C.
647 D., Eldering, A., Holz, R. E., Kuehn, R. E., and Vane, D. G., 2007: Cloud type comparisons of
648 AIRS, CloudSat, and CALIPSO cloud height and amount, Atmos. Chem. Phys. Discuss., 7,
649 13915-13958.
650 Lau, K.-M., H.-T. Wu, S. Bony, 1997: The role of large-scale atmospheric circulation in the
651 relationship between tropical convection and sea surface temperature, *J. Clim*, **10**, 381-392
652 Li, J.-L., D.E. Waliser, J.H. Jiang, D.L. Wu, W.G. Read, J.W. Waters, A.M. Tompkins, L.J.
653 Donner, J.-D. Chern, W.-K. Tao, R. Atlas, Y. Gu, K.N. Liou, A. Del Genio, M. Khairoutdinov,
654 and A. Gettelman, 2005: Comparisons of EOS MLS Cloud Ice Measurements with ECMWF
655 analyses and GCM Simulations: Initial Results, *Geophys. Res. Lett*. 32 , L18710,
656 doi:10.1029/2005GL023788.
657 Lin B., B. Wielicki, L. Chambers, Y. Hu, and K.-M. Xu, 2002: The iris hypothesis: A negative or
658 positive cloud feedback? *J. Climate*, **15**, 3-7.

659 Lin, B., B. A. Wielicki, P. Minnis, L. Chambers, K.-M. Xu, Y. Hu, and A. Fan, 2006: The effect
660 of environmental conditions on tropical convective systems observed from the TRMM
661 satellite, *J. Clim*, **19**, 5745-5761.
662 Lindzen, R. S., 1990: Some coolness concerning global warming. *Bull. Amer. Meteor. Soc*. **71**,
663 288-299.
664 Lindzen, R. S., and S. Nigam, 1987: On the role of sea surface temperature gradients in forcing
665 low level winds and convergence in the tropics. *J. Atmos. Sci*., **44**, 2418-2436.
666 Lindzen, R. S., M.-D. Chou, and A. Y. Hou, 2001: Does the Earth have an adaptive infrared iris,
667 *Bull. Am. Meteorol. Soc,* 82, 417-432.
668 Lindzen, R. S., M.-D. Chou, and A.Y. Hou, 2002: Comments on "No evidence for iris." *Bull.*
669 *Amer. Met. Soc.*, **83**, 1345-1348.
670 Liou, K.N., Q. Fu, and T.P. Ackerman, 1988: A simple formulation of the delta-four-stream
671 approximation for radiative transfer parameterizations. *J. Atmos. Sci.*, 45, 1940-1947.
672 Liou, K.-N., 2002: An Introduction to Atmospheric Radiation (second edition), Academic Press,
673 New York, 583 pp.
674 Livesey, N. J., et al., EOS MLS Version V1.5 Level 2 data quality and description document,
675 2005, available at http://mls.jpl.nasa.gov.
676 Massie, S., A. Gettelman, W. Randel, and D. Baumgardner, 2002: Distribution of tropical cirrus in
677 relation to convection, *J. Geophys. Res.*, *107*, doi:10.1029/2001JD001293, 2002.
678 McFarquhar, G. M., and A. J. Heymsfield, 1997: Parameterization of tropical cirrus ice crystal
679 size distributions and implications radiative transfer: Results from CEPEX. *J. Atmos. Sci.,* 54,
680 2187-2200.
681 Olsen, E. T., ed., AIRS/AMSU/HSB Version 4.0 Data Release User Guide, JPL Document, 2005.

682 Parkinson, C. L., 2003: Aqua: An Earth-observing satellite mission to examine water and other
683 climate variables, *IEEE Trans. Geosci. Remote Sens.*, 41 (2), 173-183.
684 Pierrehumbert, R. T., Thermostats, radiator fins, and the local runaway greenhouse, *J. Atmos. Sci*.,
685 *52*, 1784-1806, 1995.
686 Ramanathan, V., and W. Collins, 1991: Thermodynamics regulation of ocean warming by cirrus
687 clouds deduced from observations of the 1987 El Nino, *Nature*, **351**, 27-32.
688 Ramanathan V., R. D. Cess, E. F. Harrison, P. Minnis, B. R. Barkstrom, E. Ahmad, and D.
689 Hartmann, 1989: Cloud radiative-forcing and climate: Results from the Earth Radiation
690 Budget Experiment. *Science*, 243, 57-63.
691 Rapp, A., C. Kummerow, W. Berg, and B. Griffith, An evaluation of the proposed mechanism of
692 the adaptive infrared iris hypothesis using TRMM VIRS and PR measurements, *J. Climate*,
693 **18**, 4185-4194, 2005.
694 Raval, A., and V. Ramanathan, Observational determination of the greenhouse effect, *Nature,*
695 *342,* 758-762, 1989.
696 Rossow, W. B., and R.A. Schiffer, 1991: ISCCP Cloud Data Products. *Bull. Amer. Meteor. Soc*.,
697 72, 2–20.
698 Schoeberl, et al., Overview of the EOS Aura Mission, 2006: *IEEE Trans. Geosci. Remote*
699 *Sensing,* **44**, 1066-1074.
700 Schoeberl, M. R. and S. Talabac, "The Sensor Web: A future Technique for Science Return, in
701 Observing Systems for Atmospheric Composition, 2006, G. Visconti, P. DiCarlo, B.
702 Brune, M. Schoeberl, A. Wahner, Eds, Springer, NY, pgs. 203-206.
703 Soden, B. J., and R. Fu, 1995: A Satellite Analysis of Deep Convection, Upper-Tropospheric
704 Humidity, and the Greenhouse Effect, *J. Clim*, *8*, 2333-2351.

705 Soden, B. J, Broccoli A. J., and Hemler R. S., 2004: On the Use of Cloud Forcing to Estimate
706 Cloud Feedback. *J. Clim*, 17, 3661–3665.
707 Stephens, G. L., D. G. Vane, R. Boain, G. Mace, K. Sassen, Z. Wang, A. Illingworth, E.
708 O'Connor, W. Rossow, S. L. Durden, S. Miller, R. Austin, A. Benedetti, C. Mitrescu, and the
709 CloudSat Science Team, 2002: The CloudSat Mission and the A-Train: A new dimension of
710 space-based observations of clouds and precipitation. *Bull. Amer. Meteor. Soc.*, **83** (12), 1771-
711 1790.
712 Stephens, G. L. 2005: Cloud feedbacks in the climate system: A critical review. *J. Climate*, **18**,
713 237–273.
714 Su, H., W. G. Read, J. H. Jiang, J. W. Waters, D. L. Wu, and E. J. Fetzer: Enhanced positive water
715 vapor feedback associated with tropical deep convection: New evidence from Aura MLS,
716 *Geophys. Res. Lett.* 33, L05709, doi:10.1029/2005GL025505, 2006a.
717 Su, H., D.E. Waliser, J.H. Jiang, J-L. Li, W.G. Read, J.W. Waters, and A.M. Tompkins,
718 Relationships of upper tropospheric water vapor, clouds and SST: MLS observations,
719 ECMWF analyses and GCM simulations, *Geophys. Res. Lett. 33*, L22802,
720 doi:10.1029/2006GL027582, 2006b.
721 Sun, D. Z., and R. S. Lindzen, 1993: Distribution of tropical tropospheric water vapor, *J. Atmos.*
722 *Sci*., *50*, 1644-1660.
723 Sun, D. Z. and Z. Liu, Dynamic ocean-atmosphere coupling: a thermostat for the tropics. *Science*,
724 272, 1148-1150, 1996.
725 Susskind, J., C. D. Barnet, and J. M. Blaisdell, 2003: Retrieval of atmospheric and surface
726 parameters from AIRS/AMSU/HSB data in the presence of clouds, *IEEE Trans. Geosci.*
727 *Remote Sens.,* 41, 390-409.

728 Tompkins A. M., and Craig G. C., 1999: Sensitivity of Tropical Convection to Sea Surface
729 Temperature in the Absence of Large-Scale Flow. *J. Climate*: Vol. 12, No. 2 pp. 462–476.
730 Udelhofen, P. M., and D. L. Hartmann, D. L., 1995: Influence of tropical cloud systems on the
731 relative humidity in the upper troposphere, *J. Geophys. Res*., *100*, 7423-7440.
732 Waliser, D. E, N. E.Graham, and C. Gautier, 1993: Comparison of the Highly Reflective Cloud
733 and Outgoing Longwave Radiation Datasets for Use in Estimating Tropical Deep Convection.
734 *J. Clim.,* 6, 331–353.
735 Wallace, J. M., Effect of deep convection on the regulation of tropical sea surface temperature,
736 *Nature*, 357, 230-231, 1992.
737 Waters, J. W., et al., 2006: The Earth Observing System Microwave Limb Sounder (EOS MLS)
738 on the Aura satellite, *IEEE Trans. Geosci. Remote Sensing,* **44**, 1075-1092.
739 Wu, D. L., J. H. Jiang, and C. P. Davis, 2006: EOS MLS cloud ice measurements and cloudy-sky
740 radiative transfer model, *IEEE Trans. Geosci. Remote Sensing,* **44**, 1156-1165.
741 Wu, D. L., J. H. Jiang, William G. Read, et al, 2008: Validation of Aura MLS cloud ice water
742 content measurements, *J. Geophys. Res*., in press.
743 Zhang, M. H., R. D. Cess, and S. C. Xie, 1996: Relationship between cloud radiative forcing and
744 sea surface temperature over the entire tropical oceans, *J. Climate*, **9**, 1374-1384.

Table Captions

Table 1. Regression slopes (in the units of percentage change K^{-1}, relative to the long-term means) of precipitation, AIRS UT cloud fraction (CTP < 300 hPa) and MLS IWP (from 215 hPa and up) versus the cloud-weighted SST for different tropical areas.

	Precipitation	CFR	Precipitation-normalized CFR	IWP	Precipitation-normalized IWP
15ºS-15ºN	15%	13%	–2%	26%	15%
30ºS-30ºN	5%	6%	–1%	16%	10%
30ºS-30ºN, 130ºE-170ºW	7%	6%	0.1%	20%	10%

Table 2. Tropical-mean (30°S-30°N) LW, SW and net CRE (in W m^{-2}) in January 2005 for the radiative model runs for the "single-layer" case with different cloud fraction coverage estimates and for the "multi-layer" case.

	LW CRE	**SW CRE**	**Net CRE**
Single-layer case Standard run	4.74	–2.00	2.74
Single-layer case +0.2 CFR run	5.05	–2.03	3.02
Single-layer case Overcast run	21.39	–3.82	17.57
Multi-layer case Standard run	4.28	-1.44	2.84

Figure Captions

Figure 1. AIRS effective cloud fraction (color-shaded) on ascending orbit on January 27, 2005, along with MLS ascending orbit tracks (black dotted lines).

Figure 2. Scatter plots of (a) the tropical-averaged (15ºS-15ºN) CFR (CTP < 300 hPa) versus cloud-weighted SST; (b) the tropical-averaged CFR versus the tropical-averaged precipitation; (c) the tropical-averaged precipitation versus the cloud-weighted SST; and (d) the precipitation-normalized CFR (in % mm^{-1} day) versus the cloud-weighted SST. Each point is a daily value from September 1, 2002 to September 30, 2006. The solid lines are the least squares linear fits to the data, with the corresponding equations shown. The dotted line in Fig. 1b marks the regression line constrained to go through zero (see text for details).

Figure 3. Regression coefficients of AIRS CFR onto the high-pass cloud-weighted SST. The cloud-weighted SST is divided by its standard deviation.

Figure 4. Zonal averages of SST, CFR and precipitation for days when the cloud-weighted SST is less than average (solid lines) and for days when the cloud-weighted SST is greater than average (dashed lines), (a) unfiltered data; (b) high-passed data.

Figure 5. Scatter plots of tropical-averaged (15ºS-15ºN) IWC versus the cloud-weighted SST at three pressure levels, (a) 100 hPa, (b) 147 hPa and (c) 215 hPa; and (d) the MLS-derived CTP versus the cloud-weighted SST. Each point is a daily value from August 8, 2004 to September 30, 2006. The solid lines are the least squares linear fits to the data, with the corresponding equations shown.

Figure 6. Scatter plots of (a) the tropical-averaged (15ºS-15ºN) IWP (integrated from 215 hPa) versus the cloud-weighted SST; (b) the tropical-averaged IWP versus the tropical-averaged precipitation; (c) the tropical-averaged precipitation versus the cloud-weighted SST; and (d) the precipitation-normalized IWP (in g m^{-2} mm^{-1} day) versus the cloud-weighted SST. Each point is a daily value from August 8, 2004 to September 30, 2006. The solid lines are the least squares linear fits to the data, with the corresponding

778 equations shown. The dotted line in Fig. 3b marks the regression line constrained to go through zero (see
779 text for details).
780 **Figure 7**. Zonal averages of SST, IWP and precipitation for days when the cloud-weighted SST is less than
781 average (solid lines) and for days when the cloud-weighted SST is greater than average (dashed lines), (a)
782 unfiltered data; (b) high-passed data. The SST and precipitation are interpolated to the MLS IWC
783 measurement location and 2-years of data from August 2004 to September 2006 are used here.
784 **Figure** 8**.** The changes of tropical-mean CREs (a) net, (b) LW and SW (in W m^{-2}) when the tropical-mean
785 IWP is increased successively. The x-axis is the percentage increase of IWP relative to the presently
786 observed value by MLS. All results are based on the January 2005 UT cloud profiles, assuming no low and
787 middle clouds underneath.
788
789
790

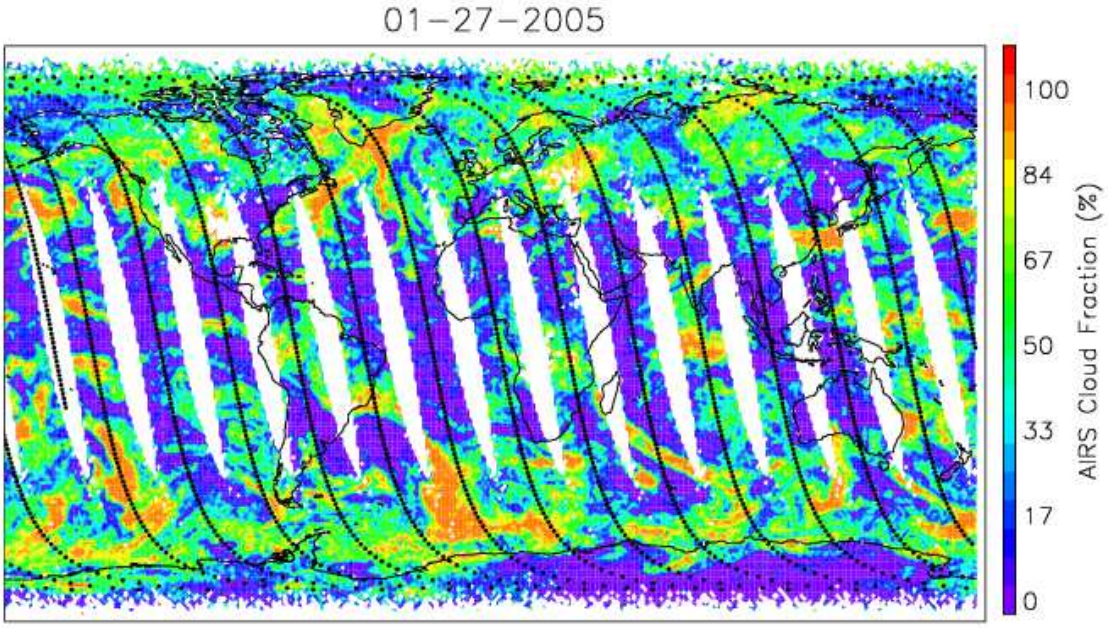

Figure 1. AIRS effective cloud fraction (color-shaded) on ascending orbit on January 27, 2005, along with MLS ascending orbit tracks (black dotted lines).

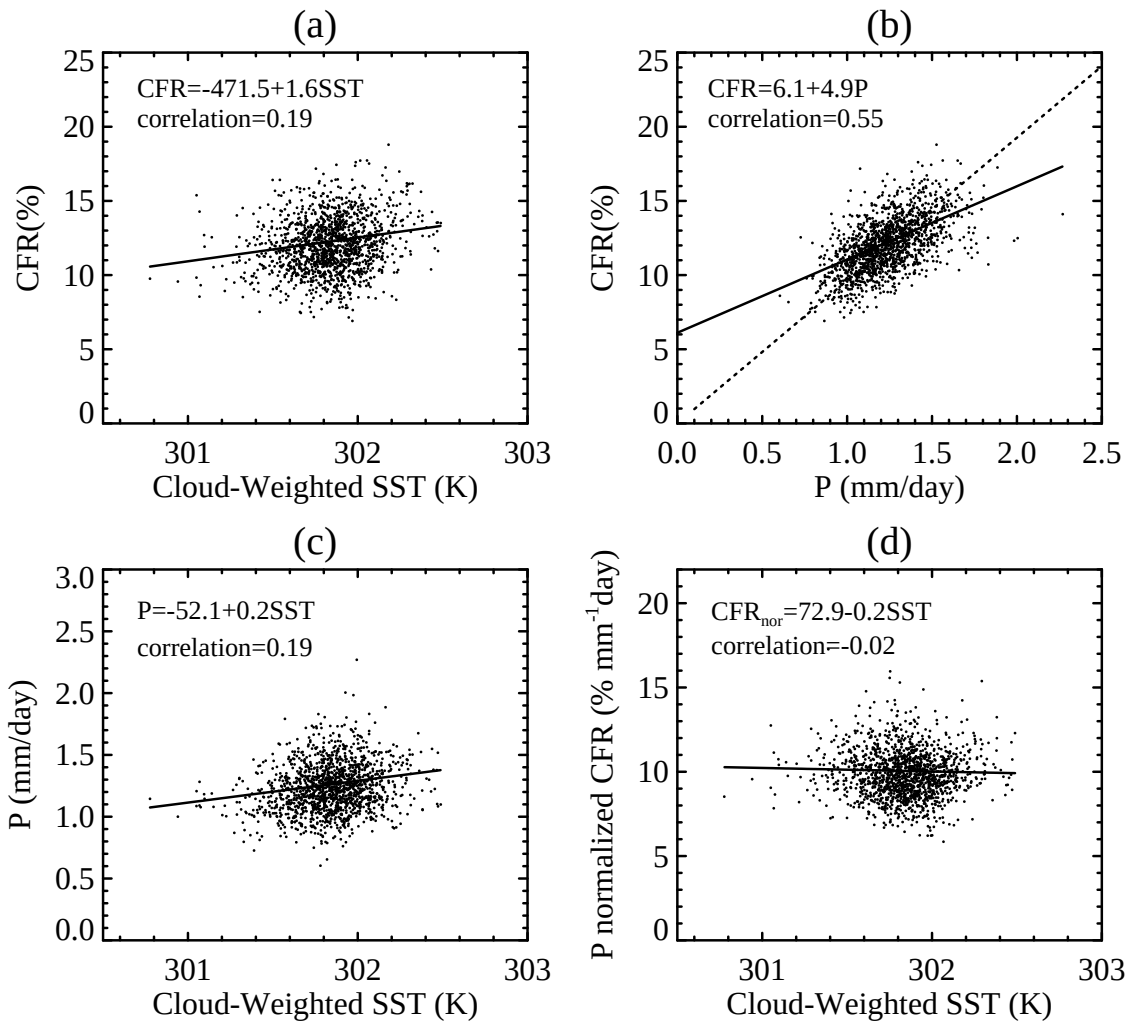

795

796 **Figure 2.** Scatter plots of (a) the tropical-averaged (15ºS-15ºN) CFR (CTP < 300 hPa) versus the cloud-
797 weighted SST; (b) the tropical-averaged CFR versus the tropical-averaged precipitation; (c) the tropical-
798 averaged precipitation versus the cloud-weighted SST; and (d) the precipitation-normalized CFR (in %
799 mm^{-1} day) versus the cloud-weighted SST. Each point is a daily value from September 1, 2002 to
800 September 30, 2006. The solid lines are the least squares linear fits to the data, with the corresponding
801 equations shown. The dotted line in Fig. 1b marks the regression line constrained to go through zero (see
802 text for details).

803

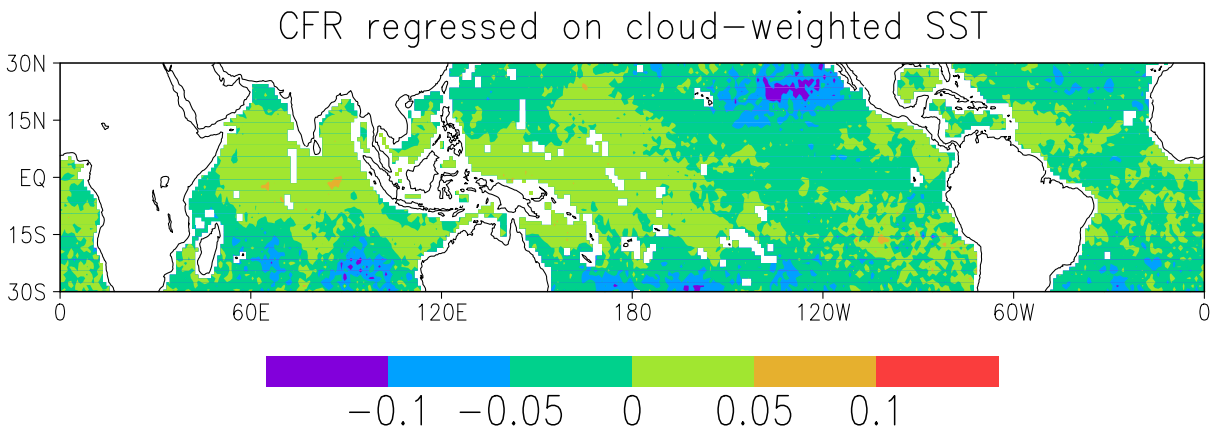

804

805 **Figure 3.** Regression coefficients of AIRS CFR onto the high-pass cloud-weighted SST. The cloud-
806 weighted SST is divided by its standard deviation.

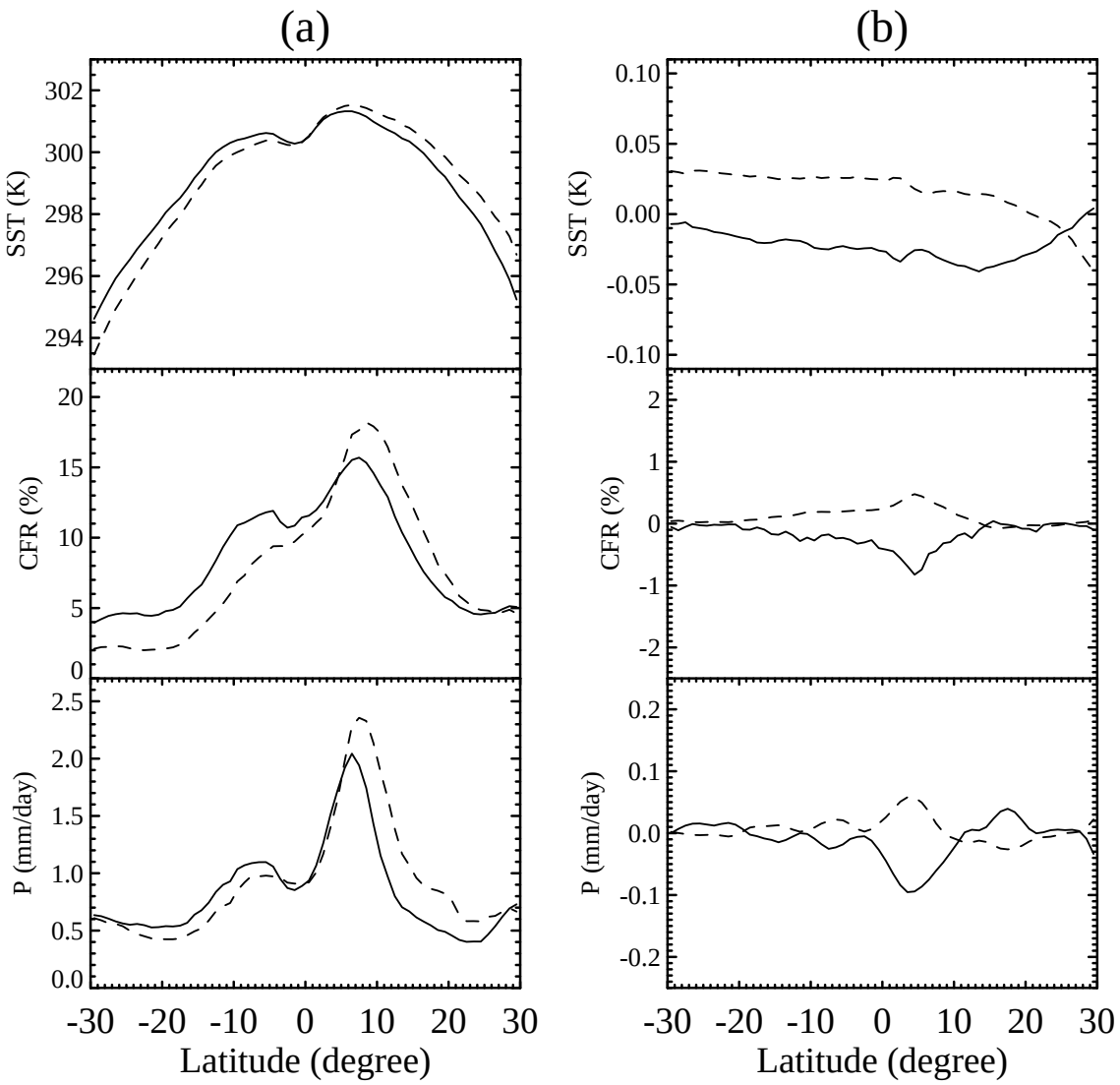

807

808

809 **Figure 4.** Zonal averages of SST, CFR and precipitation for days when the cloud-weighted SST is less than

810 average (solid lines) and for days when the cloud-weighted SST is greater than average (dashed lines), (a)

811 unfiltered data; (b) high-passed data.

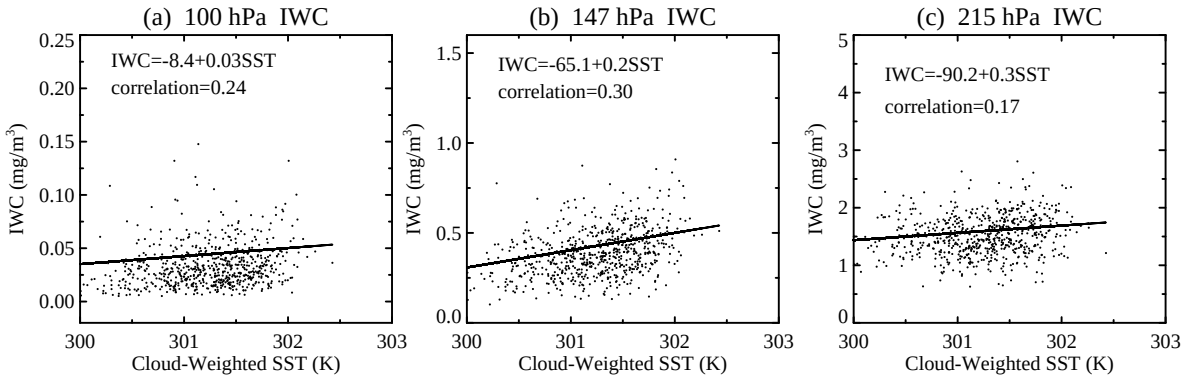

812

813 **Figure 5.** Scatter plots of tropical-averaged (15ºS-15ºN) IWC versus the cloud-weighted SST at three
814 pressure levels, (a) 100 hPa, (b) 147 hPa and (c) 215 hPa. Each point is a daily value from August 8, 2004
815 to September 30, 2006. The solid lines are the least squares linear fits to the data.

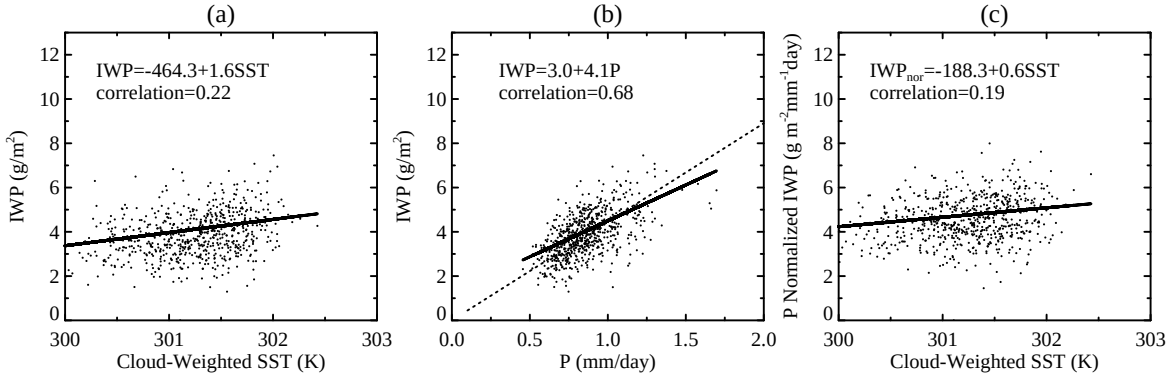

Figure 6. Scatter plots of (a) the tropical-averaged (15ºS-15ºN) IWP (integrated from 215 hPa) versus the cloud-weighted SST; (b) the tropical-averaged IWP versus the tropical-averaged precipitation; and (c) the precipitation-normalized IWP (in g m^{-2} mm^{-1} day) versus the cloud-weighted SST. Each point is a daily value from August 8, 2004 to September 30, 2006. The solid lines are the least squares linear fits to the data, with the corresponding equations shown. The dotted line in Fig. 1b marks the regression line constrained to go through zero (see text for details).

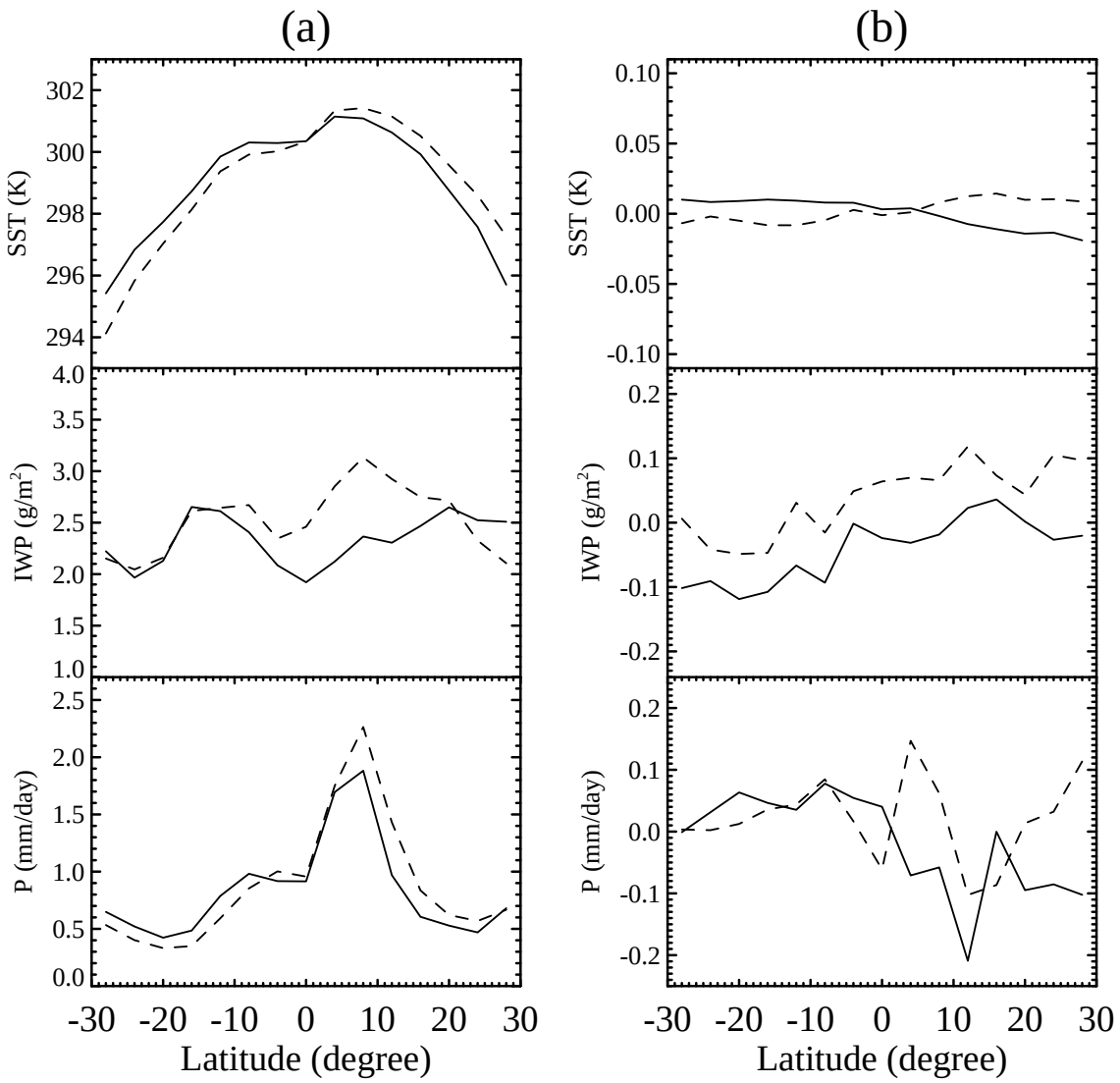

824

825 **Figure 7.** Zonal averages of SST, IWP and precipitation for days when the cloud-weighted SST is less than
826 average (solid lines) and for days when the cloud-weighted SST is greater than average (dashed lines), (a)
827 unfiltered data; (b) high-passed data. The SST and precipitation are interpolated to the MLS IWC
828 measurement location and 2-years of data from August 2004 to September 2006 are used here.

829

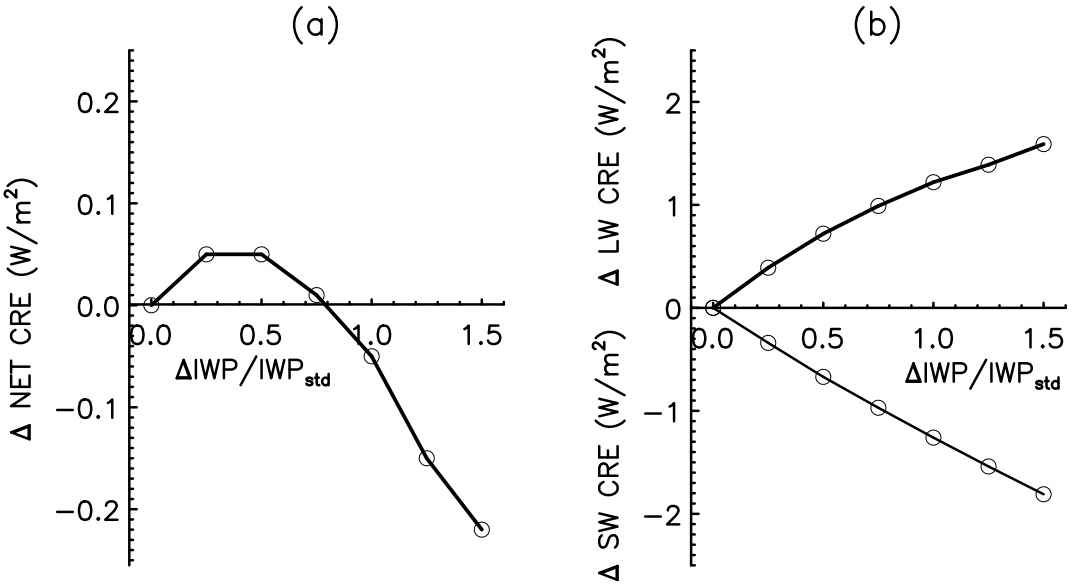

830

831 **Figure** 8**.** The changes of tropical-mean CREs (a) net, (b) LW and SW (in W m^{-2}) when the tropical-mean
832 IWP is increased successively. The x-axis is the percentage increase of IWP relative to the presently
833 observed value by MLS. All results are based on the January 2005 UT cloud profiles, assuming no low and
834 middle clouds underneath.